Reducing the cogging torque effects in hybrid stepper machines by means of resonant controllers

Antoni Arias, Jesús Caum, Edorta Ibarra and Robert Griñó, *Senior Member, IEEE*

***Abstract*—Permanent magnet machines are not free from the interaction between magnets and the stator and rotor slots, which causes an undesired disturbing torque. Such cogging or detent torque is especially larger with salient pole machines, as it is the case of the Permanent Magnet Hybrid Stepper Machines (PMHSM).**

Depending on the application requirements, these torque perturbations can be unacceptable and the application of solutions that minimizes the cogging torque effects are mandatory. This paper originally faces the minimization of the cogging torque using resonant controllers. More specifically, the paper details the analysis and design of a speed-adaptive resonant controller, which not only is directly designed in Z domain but also considers the current (or torque) inner loop delay. Pole-zero placement and the disturbance rejection frequency response have been attained in the design of the speed and position speed-adaptive controllers. Experimental results with two off-the-shelf PMHSMs demonstrate the superior performance of the proposal in both speed and position closed-loop applications for tracking, as well as in disturbance (load impact) rejection tests and against inertia variations. A comparison with a conventional PI has been carried out from the design stage to experimental results and the improvement of the proposal has been numerically quantified.

***Index Terms*—Cogging torque, resonant controller, Permanent Magnet Hybrid Stepper Machine, speed control, position control, Field Oriented Control.**

I. Introduction

Nowadays, Permanent Magnet Hybrid Stepper Machines (PMHSMs), also known as Stepper Motors (SMs), are considered as an attractive technology for position-controlled motion applications [1]–[3]. Hence, the PMHSMs presence in the market share is remarkable [4]–[7], as well as their role in numerous state-of-the-art applications. Among these endless list of applications, several works could be mentioned like [8], where the SM is a satisfactory choice for driving the control rods of a modular high temperature gas-cooled reactor. Also in [9], SMs are used to position each of the 88 intersection cells of the three undulator segments of the European X-ray Free Electron Laser. Likewise, SMs are the choice in [10] to mechanically reconfigure a novel antenna, in [11] to actuate in a spectrophotometer, in [12] to track the sun, in [13] to drive a vertical column and in [14] as a disk driver.

PMHSMs most relevant feature is the capability of performing accurate position control without the use of any electromechanical feedback sensor by means of the well-known micro-stepping technique [15]–[17]. However, such open-loop positioning technique suffers from two important inconveniences, which are, the always threatening loss of steps [18], [19] with the consequent position error, and the use of maximum current [20], which implies poor efficiency, as well as extra heating. Both of the previous inconveniences are skipped by using vector control (knwon also as Field Oriented Control) with an encoder or resolver feedback, similarly as other servo applications [21], [22]. However, when using vector control at low speeds or standstill in position control applications, the undesired cogging torque effects appear.

Cogging torque is a distorting periodic torque generated by the tendency of the rotor magnetic field to be aligned with the stator poles [23], [24]. These torque oscillations produce vibrations and additional noise and are present even if no torque production is commanded (i.e., without currents circulating through the stator). Such distorting torque is position dependent and its periodicity per revolution depends on the number of magnetic poles and the number of teeth on the stator. Therefore, the cogging torque can be treated as a periodic disturbance, whose amplitude value is almost constant, but its frequency is a multiple of the mechanical frequency of rotation.

In servo drive applications, where precise speed or position control is required, such cogging torque is almost imperceptible at medium and high speeds [25]. Some research papers claim that these values are relatively negligible compared to standard electromagnetic torques, so they can be neglected [25], [26]. However, at low speeds it can create high ripples in the mechanical speed and extra difficulties to achieve

Manuscript received March, 2018; revised May, 2018; accepted May, 2018. The present work has been supported by the Government of Spain through Projects DPI2017-85404-P and DPI2014-53685-C2-2-R of the *Ministerio de Economía y Competitividad* and FEDER funds, through Project 2017 SGR 872 of the Generalitat de Catalunya, and through Project KT4e-TRANS (KK-2015/00047 and KK-2016/00061), within the ELKARTEK program of the Government of the Basque Country. This work has also been supported by the Department of Education, Linguistic Policy and Culture of the Basque Government within the fund for research groups of the Basque university system IT978-16.

A. Arias and R. Griño are with the Institut d'Organització i Control, Universitat Politècnica de Catalunya, Av. Diagonal, 647, 08028 Barcelona, Spain (antoni.arias@upc.edu, roberto.grino@upc.edu).

J. Caum is with the Centre for Sensors Instruments and Systems Development. Universitat Politècnica de Catalunya. Rambla de Sant Nebridi, 08222 Terrassa, Spain (jesus.caum@upc.edu)

E. Ibarra is with the Department of Electronics Technology, UPV/EHU, C. Rafael Moreno Pitxitxi 3, 48013 Bilbao, Spain (edorta.ibarra@ehu.eus).

the targeted position. In many applications, such effects are unaffordable and its minimization becomes mandatory [27].

A great amount of scientific literature regarding cogging torque minimization can be found, which can be broadly divided into two approaches: (i) the ones focused on altering the physical machine design [24], [28]–[34] and (ii) the ones based on pre-commissioning processes to evaluate the cogging torque for further compensation [27], [35], [36]. Inconveniences exist in both approaches, being the most relevant the unavoidable actions to be taken before the manufacturing for the first approaches and the accurate pre-commissioning process, with the compulsory use of high resolution resolvers or encoders at some point, for the second ones.

With the aim of opening a third approach to tackle the cogging torque, this paper proposes the use of resonant controllers. Such controllers are based on the application of the Internal Model Principle [37] and, consequently, they constitute an adequate approach to the problem of tracking periodic references or, as in this case with the cogging torque, rejecting periodic disturbances with a finite number of significant harmonics. Resonant controllers [38]–[42] have been already applied, among others, to mechanical systems [43] and power electronic inverters [39], [41], [42]. In this work, however, there is the particular scenario of needing to adapt its resonant frequency as a function of the motor mechanical speed.

The paper details the analysis and design of a speed-adaptive resonance controller, which not only is directly designed in Z domain but also considers the current (or torque) inner loop delay. Pole-zero placement and disturbance rejection frequency response have been attained in the design. In order to evaluate the superiority of the proposed resonant speed-adaptive controller, a comparison with a standard PI is carried out. Finally, experimental results with two different off-the-shelf PMHSMs demonstrate the superior performance of the proposal in both speed and position tracking closed-loop applications, as well as in disturbance rejection (load impact) tests. Moreover, a higher robustness against inertia variation is experimentally corroborated.

II. PMHSM MODEL INCLUDING COGGING TORQUE

The α/β two-phase bipolar PMHSM electrical equations are written in (1) and (2) [44].

$$L\frac{di_\alpha}{dt} = v_\alpha - Ri_\alpha - \Phi_{PM}N_r\omega_m\sin(N_r\omega_m t), \quad (1)$$

$$L\frac{di_\beta}{dt} = v_\beta - Ri_\beta - \Phi_{PM}N_r\omega_m\sin(N_r\omega_m t - \frac{\pi}{2}), \quad (2)$$

where v_α, v_β, i_α and i_β are the stator voltages and currents; R and L are the stator nominal resistance and inductance; Φ_{PM} is the PM flux; ω_m is the mechanical angular speed and N_r is the PMHSM rotor teeth-number (which effectively is equivalent to the pole-pair number as in other AC machines, in the sense that it is the factor between electrical and mechanical angular speeds). The electromagnetic torque (τ) produced by the PMHSM is the interaction (or vector product) between all magnetic fluxes and currents, as follows:

$$\tau = N_r\Phi_{PM}\sin(N_r\omega_m t + \frac{\pi}{2})i_\beta - N_r\Phi_{PM}\sin(N_r\omega_m t)i_\alpha. \quad (3)$$

Despite the cogging torque ($\tau_{_C}$) should be mathematically represented in terms of the reluctance change between the coils and magnets [28], attending just at its impact in the speed loop, the following expression can be used:

$$\tau_{_C} = \sum_{j=1}^{\infty} K_{_C}^j \sin(j\omega_e t + \phi^j), \quad (4)$$

where $\omega_e = N_r\omega_m$ is the electrical angular speed, while $K_{_C}^j$ and ϕ^j stand for the amplitudes and phases respectively, of the different harmonic components. In this work and with the PMHSMs used, the most remarkable (and almost unique) component of the cogging torque is for $j = 1$. It must be pointed out that, while other approaches such as [36] require the exact knowledge of the parameters $K_{_C}^j$ and ϕ^j to fight against the cogging, the resonant based controller presented in this paper does not. Nevertheless, it is worth to mention that the most relevant value has been found to be equal to $K_{_C}^1$ = 0.175 Nm for the PMHSM further detailed in Table I.

Finally the mechanical speed is modelled in (5) as a first order system, being B and J the friction and inertia, ($\tau_{_L}$) the external load torque and (τ) and ($\tau_{_C}$) the previously defined electromagnetic and cogging torques.

$$J\frac{d\omega_m}{dt} = \tau - \tau_{_C} - \tau_{_L} - B\omega_m. \quad (5)$$

III. TORQUE CONTROL LOOP

Despite the fact that Field Oriented Control, implemented in this work, is out of the scope of this paper, it has been found that any influence in the speed loop must be carefully considered and therefore modelled in order to further face the speed controller design with warranties. In this sense, it must be pointed out that the torque dynamics correspond to a second order system with a tiny overshoot and a settling time at two percent equal to the speed loop sampling time (T). Also, it must be taken into account that the current controllers [44] have been implemented with a sampling rate 10 times faster than the speed loop. Therefore, an accurate torque loop model is a portion (m) of one speed loop sample time delay ($z^{(-1+m)}$), as it is indicated in figure 1. Since the Z transform is defined for an entire number of delays and not for a fractional portion of them, the modified Z transform (Z_m) [45] needs to be used instead.

IV. SPEED CONTROL LOOP INCLUDING THE PROPOSED RESONANT CONTROLLER

Among all speed control loop blocks, figure 1 contains the mechanical first order plant in series with an integrator, which is mathematically expressed as:

$$G'(s) = \frac{1/B}{(J/B)s+1}\,\frac{1}{s}. \quad (6)$$

Considering the data-sampled nature of the controller, the well-known zero-order hold (ZOH) transformation method

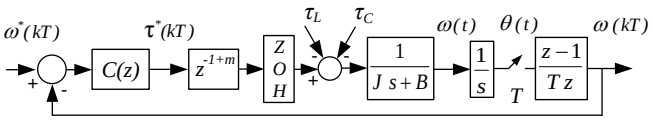

Fig. 1. Speed control loop.

TABLE I
PARAMETERS OF THE TEST BENCH.

PMHSM (reference SY57STH76-2804A)		
Parameter	**Value**	**Units**
Step angle / Phase no. / N_r	1.8 / 2 / 50	° / — / —
R / L / Voltage constant (KE)	1.13 / 3.6 / 0.524	Ω / mH / V·s·rad^{-1}
Holding / Detent Torques	1.85 / 0.067	Nm / Nm
Test bench		
Parameter	**Value**	**Units**
Total (*) Inertia / Friction	$0.3 \cdot 10^{-3}$ / $12.5 \cdot 10^{-3}$	kg·m^2 / Nm·s·rad^{-1}
Sampling period (T)	$500 \cdot 10^{-6}$	s
Encoder pulses / Speed resol.	4·2500 / 12	counts·rev^{-1} / rpm

(*) Inertia and friction include the mechanical coupling and the DC machine, i.e., are the total rig inertia and friction values.

[45], expressed in (7), has been used to obtain the plant transfer function (8) in Z domain.

$$G'(z) = (1 - z^{-1}) Z \left\{ \frac{G'(s)}{s} \right\}, \tag{7}$$

$$G'(z) = \frac{1}{B\mathrm{a}} \frac{z(\mathrm{a}T - 1 + e^{-\mathrm{a}T}) + (1 - e^{-\mathrm{a}T} - \mathrm{a}Te^{-\mathrm{a}T})}{(z-1)(z - e^{-\mathrm{a}T})}, \tag{8}$$

where $\mathrm{a} = B/J$.

On the other hand and as justified in section III, once the inner torque loop is considered as a fractional delay, the modified Z transform must be applied as stated in (9) and then (10) is obtained.

$$G_m(z) = (1 - z^{-1}) Z_m \left\{ \frac{G'(s)}{s} \right\}, \tag{9}$$

$$G_m(z) = \frac{1}{B\mathrm{a}} \frac{z^2 x_2 + z x_1 + x_0}{z(z-1)(z - e^{-\mathrm{a}T})}, \tag{10}$$

where

$x_2 = \mathrm{a}mT - 1 + e^{-\mathrm{a}mT}$,
$x_1 = 1 + \mathrm{a}T(1-m) + e^{-\mathrm{a}T}(1 - \mathrm{a}mT) - 2e^{-\mathrm{a}mT}$,
$x_0 = e^{-\mathrm{a}T}(-1 + \mathrm{a}T(-1+m) + e^{-\mathrm{a}mT})$.

The measured speed is obtained by the discrete-time derivation of the encoder measured position [21], whose transfer function is the last one on the right of figure 1. The resultant $G(z)$ plant, whose transfer function is expressed in (11), contains three poles, two of them at the origin (labelled p_3, p_4 in figure 2), a third pole (labelled p_5), whose value is equal to $e^{-\mathrm{a}T}$ and finally, two finite zeros (labelled z_3 and z_4). Specific values are fixed by the mechanical parameters, whose data is detailed in Table I.

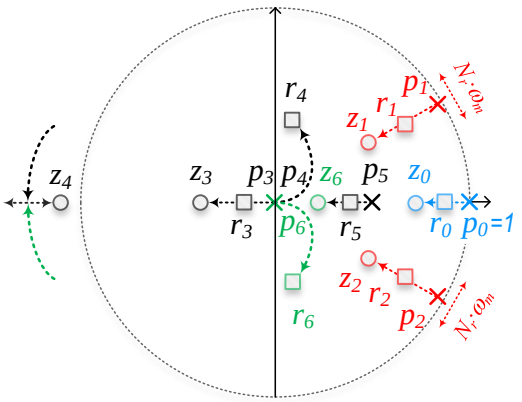

Fig. 2. Pole-zero map in Z domain and root locus evolution of the speed loop.

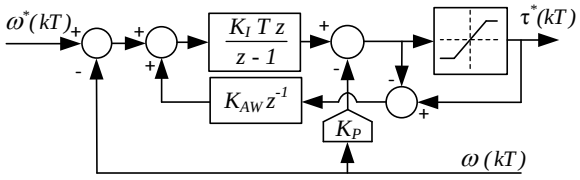

Fig. 3. Conventional Integral Proportional speed controller with the required anti-windup.

$$G(z) = G_m(z) \frac{z-1}{Tz} = \frac{1}{B\mathrm{a}T} \frac{z^2 x_2 + z x_1 + x_0}{z^2(z - e^{-\mathrm{a}T})}. \tag{11}$$

A. Conventional Proportional Integral (PI) Controller

Proportional and Integral (PI) actions combined are one of the most widespread speed controllers for electric machine commercial drives [21], [46]. In this work, the PI is tuned using (12) to fulfil the specifications of settling time at 2% ($ST_{2\%}$) and damping factor (ζ), which is fixed to 1 in order to avoid any overshoot [44].

$$K_I = \frac{5.8^2 J}{\zeta^2 ST_{2\%}^2}; \qquad K_P = \frac{5.8J}{ST_{2\%}} - B. \tag{12}$$

In order to implement it digitally, the traditional approach, valid for the majority of electric machine drives [21], [44], consists on using the backward Euler rectangular approximation:

$$\frac{1}{s} \equiv T \frac{z}{z-1}. \tag{13}$$

In this research, the IP version has been implemented instead of the conventional PI and the effect of the additional zero has been avoided without the need of a pre-filter [44], as it is shown in figure 3.

B. Proposed Resonant Integral (RI) Controller

In order to guarantee the regulation capability and the minimization of the cogging torque effect, integral $I(z)$ and

resonant $R(z)$ actions given in (14) and (15), are initially proposed.

$$I(z) = \frac{1}{z-1}. \tag{14}$$

The specifications of the resonant controller will be fixed by its poles and zeros, (labelled p_1, p_2 and z_1, z_2, respectively), indicated in (16) and (17) (and printed in red color in figure 2). Equivalently, its damping factors (ζ_z, ζ_p) and natural frequencies (ω_z, ω_p) define their behaviour. Actually, the ratio (ζ_p/ζ_z) determines the peak of attenuation, while the damping (ζ_z) fixes the width [21].

$$R(z) = \frac{1-c+d}{1-a+b}\frac{z^2-az+b}{z^2-cz+d}, \tag{15}$$

where, $a = 2e^{-T\zeta_z\omega_z}\cos\left(T\omega_z\sqrt{1-\zeta_z^2}\right)$, $b = e^{-2T\zeta_z\omega_z}$, $c = 2e^{-T\zeta_p\omega_p}\cos\left(T\omega_p\sqrt{1-\zeta_p^2}\right)$ and $d = e^{-2T\zeta_p\omega_p}$.

$$p_{1/2} = e^{-T\zeta_p\omega_p}\left[\cos\left(T\omega_p\sqrt{1-\zeta_p^2}\right) \pm j\sin\left(T\omega_p\sqrt{1-\zeta_p^2}\right)\right], \tag{16}$$

$$z_{1/2} = e^{-T\zeta_z\omega_z}\left[\cos\left(T\omega_z\sqrt{1-\zeta_z^2}\right) \pm j\sin\left(T\omega_z\sqrt{1-\zeta_z^2}\right)\right]. \tag{17}$$

As commonly done, the use of the phase-lead controller given in (18) has found to be of great help to enlarge all stability margins and therefore it has been added.

$$PL(z) = \frac{z-z_6}{z(1-z_6)}. \tag{18}$$

Since the relative degree of the initially proposed controller is 1, an additional zero (z_0) is included in the final biproper controller transfer function $C(z)$ defined in (19), which also includes a gain K. Such additional zero will have a great influence in the slowest closed-loop pole location and therefore it will fix the speed closed-loop dynamics. However, such zero might worsen the transient closed-loop response, and this is the reason for including the unity-gain pre-filter given in (20). Such pre-filter not only is designed to cancel the zero (z_0), but also to introduce a zero at the origin since it aids to damp and stabilize the speed and position closed-loops, respectively.

$$C(z) = \left(\frac{z-z_6}{z(1-z_6)}\right)K\left(\frac{z-z_0}{z-1}\right)\left(\frac{1-c+d}{1-a+b}\right)\left(\frac{z^2-az+b}{z^2-cz+d}\right), \tag{19}$$

$$PF(z) = \frac{z(1-z_0)}{z-z_0}. \tag{20}$$

The open-loop transfer function is detailed in (21) and its pole-zero map, together with the root locus, are illustrated in figure 2, where the closed-loop poles are labelled as $r_0, r_1, r_2, r_3, r_4, r_5$ and r_6.

$$L(z) = C(z)\cdot G(z) = K'\frac{z-z_3}{p_3p_4(z-p_5)}\frac{z-z_6}{z(1-z_6)}\frac{z-z_0}{z-1}\frac{z-Rz_{1/2}\pm jIz_{1/2}}{z-Rp_{1/2}\pm jIp_{1/2}}. \tag{21}$$

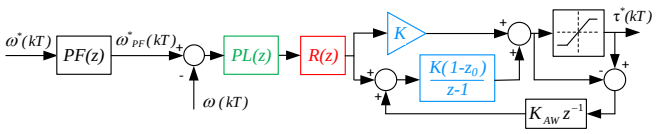

Fig. 4. Proposed speed controller with the pre-filter (PF), the phase-lead (PL), the resonant (R) and the separated integral part with its anti-windup.

A saturation in the reference torque is unavoidable and therefore an anti-windup in the integral part is also required. The final implemented controller responds to the structure mathematically detailed in (22) and schematically represented in figure 4. With this structure, it has been found that the integral part has no numerical errors since the coefficient 1 of the integrator is not further multiplied by any other number and therefore not numerically altered.

$$C(z) = \frac{z-z_6}{z(1-z_6)}\frac{1-c+d}{1-a+b}\frac{z^2-az+b}{z^2-cz+d}K\left(\frac{1-z_0}{z-1}+1\right). \tag{22}$$

It must be pointed out that $R(z)$, defined in (15), is adaptive and its four coefficients (a, b, c and d) need to be updated according to:

$$\omega_p = \omega_z = \frac{1\cdot 50\cdot\omega^*_{PF}(kT)}{\sqrt{1-2\zeta_p^2}}, \tag{23}$$

where factors 1 and 50 are justified in (4) and given in Table I, respectively. Despite the natural frequency (ω_p) is not the resonant frequency ($\omega_r = \omega_p\sqrt{1-2\zeta_p^2}$) [45], given the small value of the selected damping factor for the poles (ζ_p=0.01), they could be considered to be the same.

C. RI and PI tuning and discussion

The accurate tuning of the speed controller strongly depends on the mechanical plant parameters, where the most relevant ones are listed on Table I.

The sensitivity transfer function has a paramount importance when evaluating the effectiveness of the cogging torque rejection. In order to evaluate the superior performance of the proposed RI controller, a comparison with the well-established PI controller has been carried out all over the investigation, from the early design up to the last experimental result. In order to achieve a "fair comparison", the criteria of having the same sensitivity transfer function (24) at low frequencies has been adopted when tuning both controllers.

$$\frac{\omega(z)}{\tau_C(z)} = \frac{G'(z)(z-1)/(Tz)}{1+L(z)}. \tag{24}$$

These equivalences are infinite and among them, the values indicated in Table II have been considered for this case study. The resultant sensitivity Bodes are compared in figure 5, where the frequency responses are almost the same but in the resonant peak, which needs to vary according to the frequency component of the cogging torque. Figure 5 corresponds to a mechanical speed equal to 6 rpm, which implies (considering

TABLE II
RI AND PI TUNING PARAMETERS.

Controller	Parameters
RI	z_6=0.7 z_0=0.98 K= 0.03 ζ_p=0.01 ζ_z=0.9 $\omega_p = \omega_z = \frac{\omega^*_{PF}(kT)\cdot 50}{\sqrt{1-2\zeta_p^2}}$
PI	$ST_{2\%}$ = 90 ms ζ=1

the factor 50) that the attenuation peak is placed at $2\pi\cdot5$ rad/s with a gain of -12.8 dB; -39 dB less than the PI; which is imposed by the ratio (ζ_p/ζ_z) as follows:

$$20\,log_{10}\frac{0.01}{0.9} = -39dB. \tag{25}$$

The adaptation of the resonant controller to track the cogging perturbation in accordance with the speed has a direct impact in all the pole-zero map. Therefore, not only the poles from the resonant controller vary, but also all six closed-loop poles do. Special care should be taken when dealing with the actual plant. In fact, the lower the inertia, the more difficult of the resonant tuning may become. In this sense, it must be pointed that:

1) Reducing the overall controller RI gain K from (19) may eventually be useful.
2) At high speeds, the closed-loop poles r_4 and r_6 (figure 2) travel very rapidly outside the unitary circle. However, at such speeds, the cogging torque is filtered by the mechanical plant itself and eventually its effects in the speed become unnoticeable. The adopted practical solution has been to adapt ω_p and ω_z up to a certain, experimentally found, speed threshold (around 150 rpm in this work), after which the resonant controller is no longer updated. In other words, the adapting process works within the positive and negative speed threshold inside which the cogging torque becomes noticeable.
3) The introduction of the phase-lead controller defined in (18) enlarges such speed threshold. Outside this range, the proposed controller works with a fixed resonant and therefore equivalently as the PI.

Finally, it should be remarked the importance of the branch defined by the zero z_0 and the integrator open-loop pole p_0, since such branch contains the slowest closed-loop pole r_0, who fixes the dynamics (figure 2). Moreover, with the introduction of the pre-filter, given in (20) and illustrated in figure 4, any influence of the nearby zero z_0 is totally cancelled.

V. Position Control Loop

Figure 6 illustrates the position loop, composed by the inner speed closed-loop and the $Cp(z)$ as a position controller, which is just a proportional gain for both (RI and PI) options. This position loop scheme has the measured sampled position in the feedback path and consequently it must be considered in the open-loop transfer function (26). With $Cp(z) = 2$, a good performance, in the double sense of achieving smooth motion

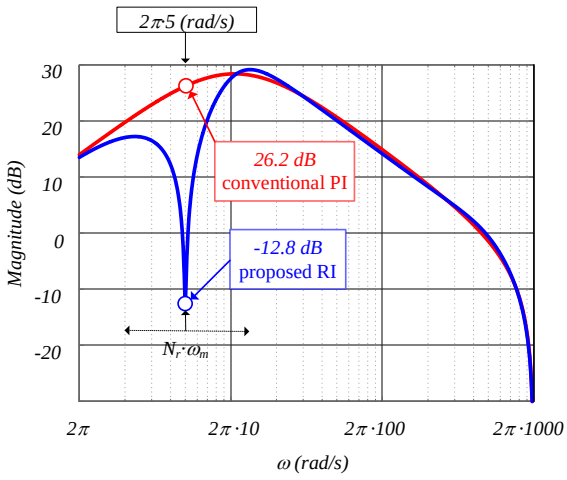

Fig. 5. Sensitivity Bode for conventional PI (red) and proposed RI (blue) when n^*_m= 6 rpm and the resonant attenuation peak is at 5 Hz.

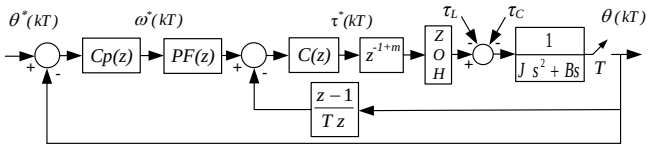

Fig. 6. Position control loop.

during the tests and obtaining an illustrative comparison with both RI and PI controllers, has been achieved.

$$Lp(z) = Cp(z)PF(z)\frac{(L(z)Tz)/(z-1)}{1+L(z)}. \tag{26}$$

VI. Experimental Results

Figure 7 ilustrates the four-quadrant experimental rig, which consists of a DC motor to emulate any type of load, the off-the-shelf PMHSM (reference SY57STH76-2804A [7]) and the Texas Instruments TMS320F28335 (150 MHz floating point) Digital Signal Controller (DSC).

Reference tracking and disturbance rejection are the two main tests to evaluate the performance of any controller. Consequently, three test types have been carried out: load impact and speed and position closed-loop controls. An encoder of 10000 pulses per revolution has been used, which implies a speed resolution of 12 rpm, justified in (27). Such inherent ripple appears all over the speed waveforms.

$$12\,(rpm) = \frac{\Delta\theta}{T} = \frac{1\,(pulse)}{0.5\cdot10^{-3}\,(s)}\frac{60\,(s)}{1\,(min)}\frac{1\,(rev)}{10^4\,(pulse)}. \tag{27}$$

A. Load Impact

Instead of dealing with a step, as usually done, it has been considered much more appropriate to test the load impact against a periodic disturbance, since its rejection is the main goal of the RI controller. Hence, during such test, the DC

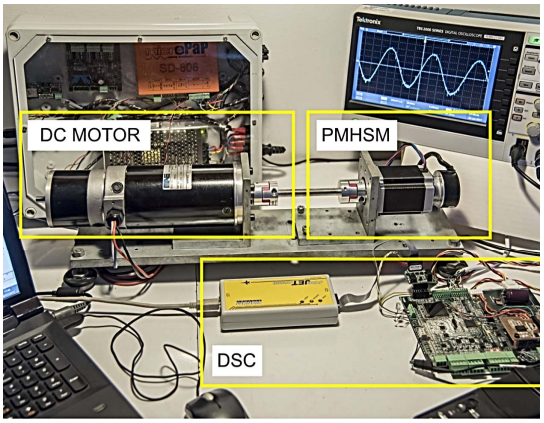

Fig. 7. Experimental rig composed by the PMHSM, DC MOTOR with its drive and the Digital Signal Controller with the power converter on the right.

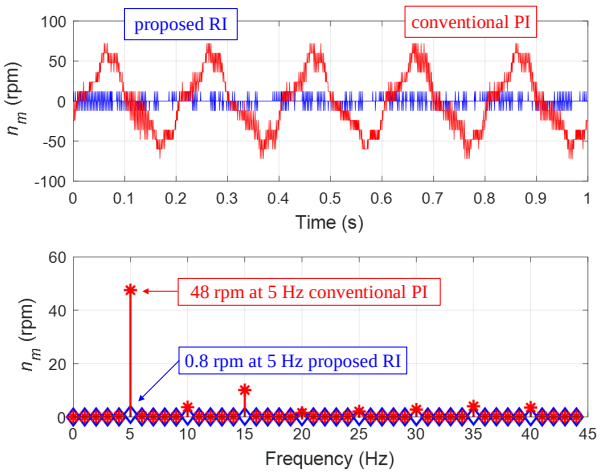

Fig. 8. Sinusoidal load impact disturbance rejection comparison for the proposed RI (blue) versus the conventional PI (red) and their FFTs.

motor is driven in closed-loop torque control with a sinusoidal reference of constant amplitude and constant frequency. Actually, the low speed scenario has been selected since it is when the unwanted cogging torque influence becomes stronger. Specifically, a frequency for the DC motor sinusoidal torque reference of 5 Hz has been chosen, which would correspond to the main cogging torque component when the machine would rotate as slow as 6 rpm ($fe = n_m(rpm)\frac{N_r}{60}$). On the other hand, the PMHSM is in speed closed-loop control with a reference value equal to 0 rpm and therefore fighting to keep the rotor at zero speed. Figure 8, which illustrates the mechanical speed $n_m(rpm)$ and their FFTs for the RI and PI controllers, shows the excellent and much superior performance of the former. Also in figure 8, the harmonic component attenuation at 5Hz is reduced from 48 rpm to 0.8 rpm, which corresponds to -35.5 dB (where the theoretical value was -39 dB as illustrated in figure 5).

With this test, the application of resonant controllers to mitigate periodic load impact perturbations under steady-state conditions has been positively demonstrated. Also, it has been experimentally corroborated that the reduction of the tuning factor ζ_p further attenuates the disturbance. However, extreme low values of ζ_p makes the resonant controller very effective at steady state, but less effective under speed control and position control where the speed varies.

B. Speed Loop

The lower the speeds, the higher becomes the challenge to mitigate the unwanted speed oscillations due to the cogging torque. Speeds of 6, 12, 18 and 24 rpm have been chosen in figures 9 to 12, because their first harmonic components lie in the exact values of 5 ,10 , 15 and 20 Hz, respectively. Hence, all FFTs shown are much cleaner and of easier comparison. It is relevant to point out that the steady state speed figure appears in the DC component of the FFTs. Table III shows the calculated THD for the first 44 components, as indicated in the following expression:

TABLE III
TOTAL HARMONIC DISTORTION (THD) AND COGGING COMPARISONS OF FIGURES 9 TO 12 FFTS FOR THE PROPOSED RI VERSUS THE CONVENTIONAL PI.

	THD			Cogging			
Speed rpm	RI -	PI -	Att. %	Comp. Hz	RI rpm	PI rpm	Att. dB
6	5.57	9.97	178.9	5	0.18	10.02	34.91
12	2.15	6.48	301.4	10	0.27	13.45	33.94
18	0.81	3.97	490.1	15	0.11	12.20	40.89
24	0.49	2.58	526.5	20	0.24	13.70	35.13

$$THD = \sum_{Freq=1(Hz)}^{44(Hz)} \frac{n_m(rpm)_{Freq}}{n_m(rpm)_{DC}}. \quad (28)$$

The overall improvement obtained by the proposed RI when compared to the conventional PI is clearly confirmed in time and frequency domains, as well as with the numerical computed values from the FFTs given in Table III. Also, from the same Table III, it can be concluded that the cogging disturbance component (Comp.) is perfectly rejected for all speeds by the proposed RI and the calculated attenuation (Att.) matches reasonably well with the theoretical -39 dB of the previously mentioned figure 5.

However, despite the overall better performance of the proposed RI, the second harmonic component is not always of lower value. Actually, in figures 10 and 11, the second harmonic components, which lie in 20 and 30 Hz respectively, are of larger value in the RI. A possible solution would be to include another resonant controller tuned to cancel it.

C. Position Loop

Position control is somehow the most difficult test to be handled by the RI controller since the speed is constantly changing and so does the resonant controller. Resonant coefficients

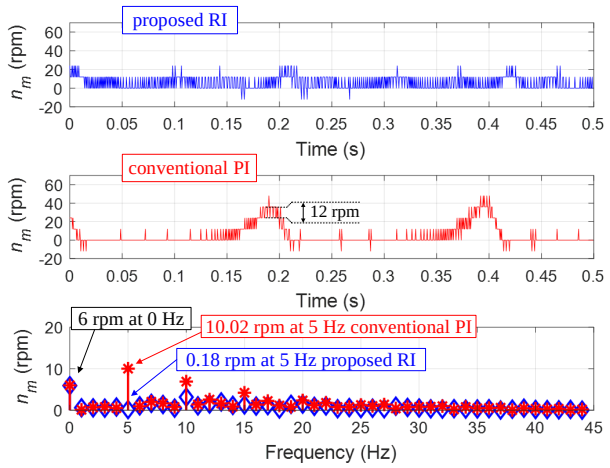

Fig. 9. Tracking 6 rpm comparison.Time waveforms and their FFTs (proposed RI in blue and conventional PI in red).

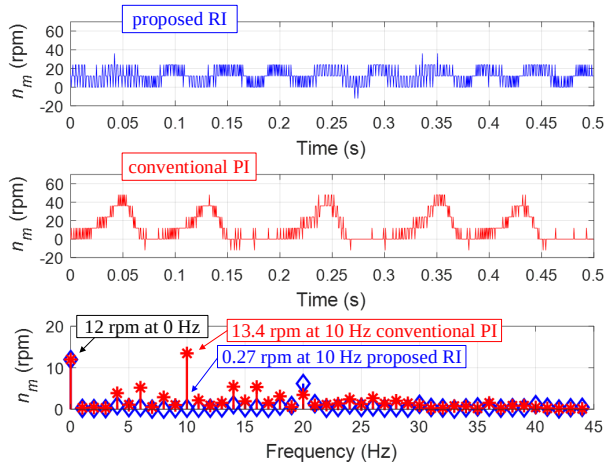

Fig. 10. Tracking 12 rpm comparison. Time waveforms and their FFTs (proposed RI in blue and conventional PI in red).

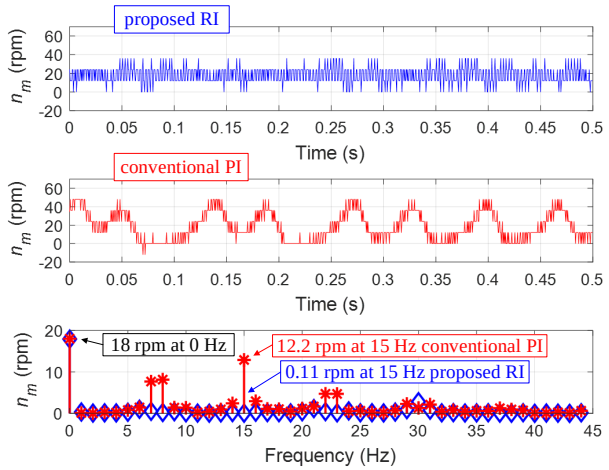

Fig. 11. Tracking 18 rpm comparison. Time waveforms and their FFTs (proposed RI in blue and conventional PI in red).

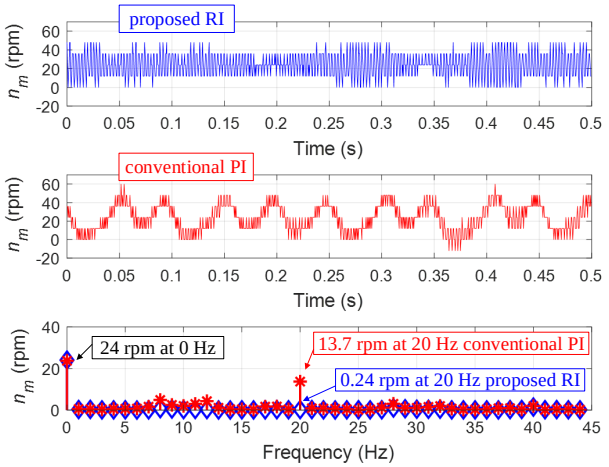

Fig. 12. Tracking 24 rpm comparison. Time waveforms and their FFTs (proposed RI in blue and conventional PI in red).

cannot be updated with the measured speed, since it would be a loop inside a loop, and instead they are updated with the reference value (pre-filtered to emulate the closed-loop dynamics). Despite all the previous, the results are of superior performance for the proposed RI , as it can bee seen in figure 13, where there has been a step change from -1000 to +1000 encoder counts and the last 1000 counts are illustrated. The 12 rpm encoder resolution clearly further perturbs the position closed-loop. Actually, the measured position is not in its final value yet, since with the adopted value of $Cp(z) = 2$, speed reference figures when approaching the position reference are so tiny. For example, when the error in encoder counts $E_\theta(counts)$ is equal to 10, the speed reference, according to (29), would be as tiny as 0.12 rpm.

$$n_m^*(rpm) = E_\theta(counts) \cdot \frac{1(rev)}{10^4(counts)} \cdot \frac{60(s)}{1(min)} \cdot Cp = \\ = E_\theta(counts) \cdot 120 \cdot 10^{-4}. \quad (29)$$

Actually, such low value of $Cp(z)$ has been chosen in order to get an exponential position waveform with a slow time constant and therefore, maximize the duration of both (i) tiny reference speeds and (ii) unwanted cogging torque disturbances.

D. Robustness against inertia (J) variation

In PMHSM drives the variation of the inertia (J) is likely to happen as in other servo motor applications. Several tests with the original rig (i.e. with the same inertia) but tuning both (proposed RI and conventional PI) controllers with different inertia values have been undertaken. Extreme J values, ($0.05 \cdot 10^{-3}$ and $0.5 \cdot 10^{-3}$ in kg·m^2) are illustrated in figures 14 and 15, respectively, and it can be concluded that robustness against inertia variation is much superior for the proposed RI than the conventional PI. Also, cogging reduction in the proposed RI is maintained and the tracking performance of the conventional PI is deeply deteriorated while the proposed RI is not.

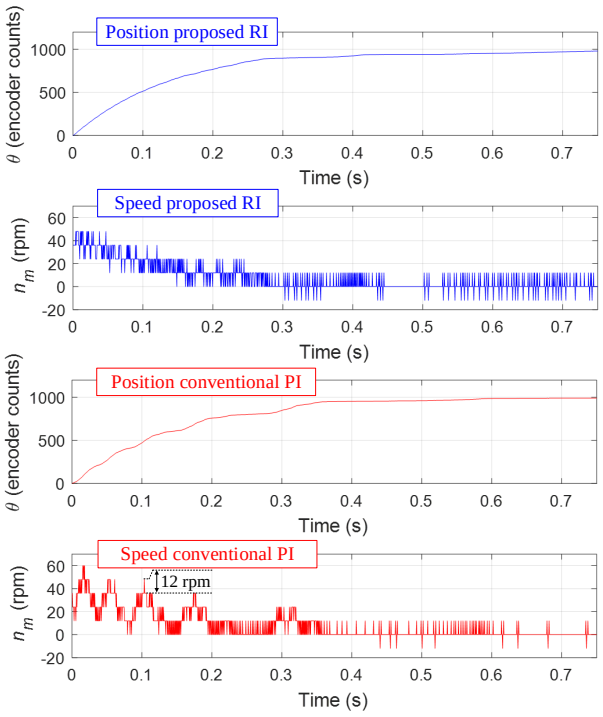

Fig. 13. Position closed-loop step response at 1000 in encoder counts comparison. Position and speed time responses (proposed RI in blue and conventional PI in red).

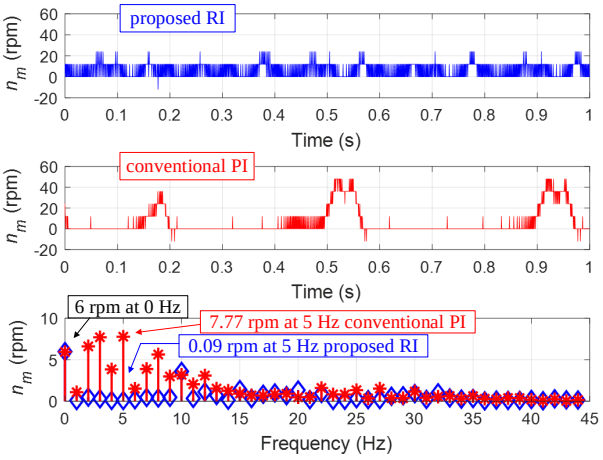

Fig. 14. Tracking 6 rpm against inertia variation ($J = 0.05 \cdot 10^{-3}$ kg·m^2). Time waveforms and their FFTs (proposed RI in blue and conventional PI in red).

VII. Extension to other PMHSMs

In order to validate the proposed resonant controller with other PMHSMs, the same experimental speed and position tests have been repeated with a second PMHSM detailed in Table IV.

The same controller parameters as in Table II are used, with two exceptions: (i) the damping of the poles ζ_p is equal to 0.001, which implies an additional -20 dB at the resonance peak, and (ii) the overall controller RI gain K has been set to 0.08 in order to meet the equivalent performance in the sensitivity function. Moreover, the ripple in the speed

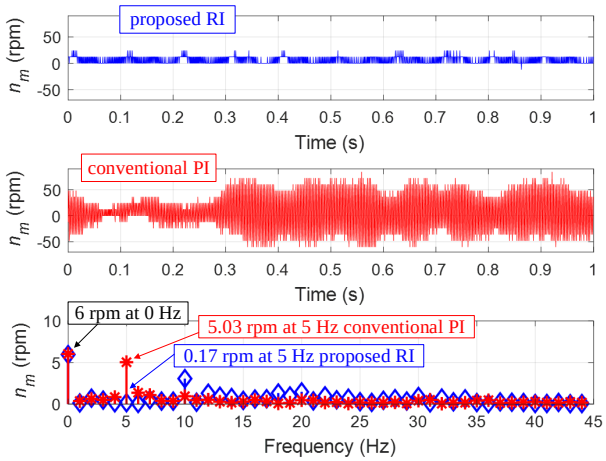

Fig. 15. Tracking 6 rpm against inertia variation ($J = 0.5 \cdot 10^{-3}$ kg·m^2). Time waveforms and their FFTs (proposed RI in blue and conventional PI in red).

TABLE IV
Parameters of the second test bench.

PMHSM (reference SY86STH118-6004B)		
Parameter	**Value**	**Units**
Step angle / Phase no. / N_r	1.8 / 2 / 50	° / — / —
R / L / Voltage constant (KE)	4.0 / 0.5 / 0.916	Ω / mH / V·s·rad^{-1}
Holding / Detent Torques	8.0 / not specified	Nm / Nm
Test bench		
Parameter	**Value**	**Units**
Inertia / Friction	$0.64 \cdot 10^{-3}$ / $54.2 \cdot 10^{-3}$	kg·m^2 / Nm·s·rad^{-1}
Sampling period (T)	$500 \cdot 10^{-6}$	s
Encoder pulses / Speed resol.	4·1000 / 30	counts·rev^{-1} / rpm

measurement is equal to 30 rpm (instead of 12) due to the new 4000 encoder pulses as indicated in Table IV.

Table V summarizes the speed results while the position test is illustrated in figure 16. Higher levels of cogging attenuation (48.07 dB at 24 rpm) are achieved, which is consistent with the fact of having a larger damping value (ζ_p=0.001) of the resonant poles. It can be concluded the superior performance of the proposed resonant controller compared to the conventional PI for this second PMHSM.

VIII. Conclusions

A different approach to minimize the cogging torque in hybrid stepper machines, based on the use of resonant controllers, has been proposed. The proposed controller, composed by a speed-adaptive resonant controller as well as an integrator, has proved to be a good choice for mitigating or eventually rejecting the cogging torque and minimizing its undesired consequences.

A Z domain comprehensive analysis based on the pole-zero placement technique and sensitivity function frequency response has been detailed. The challenge of adapting the resonance frequency of the resonant controller in accordance

TABLE V
TOTAL HARMONIC DISTORTION (THD) AND COGGING COMPARISONS FOR THE PROPOSED RI VERSUS THE CONVENTIONAL PI FOR THE SECOND PMHSM.

	THD			Cogging			
Speed rpm	RI -	PI -	Att. %	Comp. Hz	RI rpm	PI rpm	Att. dB
6	4.83	11.64	240.1	5	0.39	10.78	28.83
12	1.22	6.35	520.5	10	0.23	17.11	37.43
18	0.38	5.88	1547	15	0.09	19.08	46.52
24	0.22	2.08	945.4	20	0.09	22.80	48.07

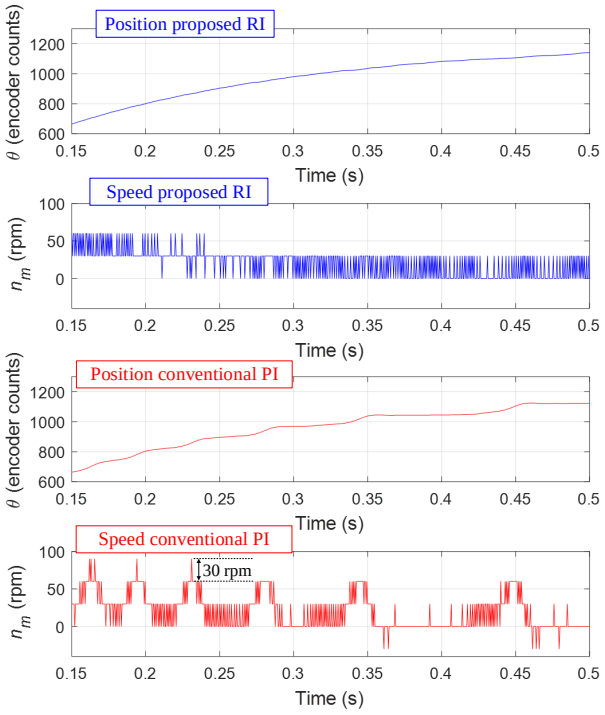

Fig. 16. Position closed-loop step response at 1200 in encoder counts comparison for the second PMHSM. Position and speed time responses (proposed RI in blue and conventional PI in red).

with the cogging disturbance torque frequency, which is a multiple of the mechanical speed, has been achieved.

A four quadrant workbench composed by an off-the-shelf Permanent Magnet Hybrid Synchronous Machine (PMHSM) attached to DC Motor has been built and a comparison of the proposed controller against a conventional PI based one, both implemented in the same 32-bit floating-point digital signal controller, has been carried out. As a result, a set of tracking and disturbance rejection experimental tests has been obtained, which illustrates the superior performance not only in low and zero closed-loop speed control, but also in closed-loop position control as well as against inertia parameter variations.

Despite the proposed control algorithm has been experimentally tested for two different PMHSMs, the authors believe that this methodology can be used with success in other AC machines, where the relation between the cogging torque and mechanical frequencies are much lower than 50 (as in the PMHSMs) and therefore it would be more favourable.

REFERENCES

[1] T. Kenjo and A. Sugawara, *Stepping Motors and their microprocessor controls*. Oxford University Press, 1994.

[2] P. Acarnley, *Stepping Motors: a guide to theory and practice*. The Institute of Electrical Engineers, 2002.

[3] B. Robert and M. Feki, *Control of Non-conventional Synchronous Motors. Chapter 9. Control of the Stepping Motor*, J. P. Louis, Ed. Wiley, 2012.

[4] Leadshine Technology Co. Ltd. [Online]. Available: http://www.leadshine.com/

[5] Nanotec Electronic GmbH & Co. KG. [Online]. Available: https://en.nanotec.com/

[6] Sanyo Denki America, Inc. [Online]. Available: http://www.sanyo-denki.com//

[7] Changzhou Songyang Machinery & Electronics Co., Ltd. [Online]. Available: http://www.cnsoyo.com/

[8] Z. Dong, "Nonlinear power-level control design for MHTGRs by considering stepper motor dynamics," *Progress in Nuclear Energy*, vol. 78, Supplement C, pp. 216–230, 2015.

[9] P. Concha and C. Vázquez, "Thermal analysis of the european XFEL intersection control rack," *IEEE Transactions on Nuclear Science*, vol. 61, no. 2, pp. 824–829, 2014.

[10] S. Basbug, "Design and synthesis of antenna array with movable elements along semicircular paths," *IEEE Antennas and Wireless Propagation Letters*, vol. 16, pp. 3059–3062, 2017.

[11] P. Visconti, A. Lay-Ekuakille, P. Primiceri, G. Ciccarese, and R. de Fazio, "Hardware design and software development for a white LED-based experimental spectrophotometer managed by a PIC-based control system," *IEEE Sensors Journal*, vol. 17, no. 8, pp. 2507–2515, 2017.

[12] A. Cappelletti, M. Catelani, L. Ciani, M. K. Kazimierczuk, and A. Reatti, "Practical issues and characterization of a photovoltaic/thermal linear focus 20× solar concentrator," *IEEE Transactions on Instrumentation and Measurement*, vol. 65, no. 11, pp. 2464–2475, 2016.

[13] J. M. Chambers and N. M. Wereley, "Vertical axis inductance monitoring system to measure stratification in a column of magnetorheological fluid," *IEEE Transactions on Magnetics*, vol. 53, no. 1, pp. 1–5, 2017.

[14] X. Chen and Y. He, "Novel programmable passive intermodulation generator using nonlinear rotating disk," *IEEE Microwave and Wireless Components Letters*, vol. 27, no. 10, pp. 945–947, 2017.

[15] W. Kim, D. Shin, and C. C. Chung, "Microstepping using a disturbance observer and a variable structure controller for permanent-magnet stepper motors," *IEEE Transactions on Industrial Electronics*, vol. 60, no. 7, pp. 2689–2699, 2013.

[16] W. Kim, D. Shin, Y. Lee, and C. C. Chung, "Simplified torque modulated microstepping for position control of permanent magnet stepper motors," *Mechatronics*, vol. 35, Supplement C, pp. 162–172, 2016.

[17] D. R. Gaan, M. Kumar, and S. Sudhakar, "Frequency modulation based microstepping of stepper motor for real time position tracking applications," in *Proc. of the IEEE International Conference on Power Electronics, Drives and Energy Systems (PEDES)*, 2016, pp. 1–6.

[18] S. Moon and D. H. Kim, "Step-out detection and error compensation for a micro-stepper motor using current feedback," *Mechatronics*, vol. 24, no. 3, pp. 265–273, 2014.

[19] K. Balakrishnan, B. Umamaheswari, and K. Latha, "Identification of resonance in hybrid stepper motor through measured current dynamics in online for accurate position estimation and control," *IEEE Transactions on Industrial Informatics*, vol. 9, no. 2, pp. 1056–1063, 2013.

[20] A. Antonioli, M. Antoniol, S. Calligaro, and R. Petrella, "A low cost sensorless drive for hybrid stepper motors based on back-EMF observer and d-axis current injection for industrial labelling machines," in *Proc. of the IEEE Applied Power Electronics Conference and Exposition (APEC)*, March 2014, pp. 2492–2499.

[21] S. N. Vukosavic, *Digital Control of Electrical Drives*. Springer, 2007.

[22] W. Kim, C. Yang, and C. C. Chung, "Design and implementation of simple field-oriented control for permanent magnet stepper motors without dq transformation," *IEEE Transactions on Magnetics*, vol. 47, no. 10, pp. 4231–4234, 2011.

[23] L. Xiao, J. Li, R. Qu, Y. Lu, R. Zhang, and D. Li, "Cogging torque analysis and minimization of axial flux PM machines with combined rectangle-shaped magnet," *IEEE Transactions on Industry Applications*, vol. 53, no. 2, pp. 1018–1027, 2017.

[24] W. Fei and P. Luk, "A new technique of cogging torque suppression in direct-drive permanent magnet brushless machines," *IEEE Transactios on Industry Applications*, vol. 46, no. 4, pp. 1332–1340, 2010.

[25] Y. Lee, D. Shin, W. Kim, and C. C. Chung, "Nonlinear H_2 control for a nonlinear system with bounded varying parameters: Application to PM stepper motors," *IEEE/ASME Transactions on Mechatronics*, vol. 22, no. 3, pp. 1349–1359, 2017.

[26] M. Butcher, A. Masi, R. Picatoste, and A. Giustiniani, "Hybrid stepper motor electrical model extensions for use in intelligent drives," *IEEE Transactions on Industrial Electronics*, vol. 61, no. 2, pp. 917–929, 2014.

[27] M. Piccoli and M. Yim, "Anticogging: Torque ripple suppression, modeling, and parameter selection," *The International Journal of Robotics Research*, vol. 35, no. 1-3, pp. 148–160, 2016.

[28] C. Hsiao, S. Yeh, and J. Hwang, "A novel cogging torque simulation method for permanent-magnet synchronous machines," *Energies*, vol. 4, pp. 2166–2179, 2011.

[29] T. Kim and J. Chang, "Effective step-skew method for cogging torque reduction in surface-mounted permanent magnet synchronous motor," *Journal of the Korean Physical Society*, vol. 63, no. 3, pp. 288–292, 2013.

[30] X. Ge, Z. Zhu, G. Kemp, D. Moule, and C. Williams, "Optimal step-skew methods for cogging torque reduction accounting for three-dimensional effect of interior permanent magnet machines," *IEEE Transactions on Energy Conversion*, vol. 32, no. 1, pp. 222–232, 2017.

[31] Z. Han, J. Liu, C. Gong, and J. Lu, "Influence mechanism on vibration and noise of PMSM for different structures of skewed stator," in *Proc. of the International Conference on Electrical Machines and Systems (ICEMS)*, 2017.

[32] Y. Ueda, H. Takahasi, A. Ogawa, T. Akiba, and M. Yoshida, "Cogging-torque reduction of transverse-flux motor by skewing stator poles," *IEEE Transactions on Magnetics*, vol. 52, no. 7, 2016.

[33] S. Lee, K. Jung, S. Chai, and J. Hong, "Cogging torque reduction in surface-mounted permanent magnet synchronous motor by axial pole pairing," in *in Proc. of the EVS28 International Electric Vehicle Symposium and Exhibition*, 2015.

[34] D. Hanselman, "Effect of skew, pole count and slot count on brushless motor radial force, cogging torque and back EMF," in *Proc. of the Electric Power Applications Conference*, 1997, pp. 325–330.

[35] K. Nakamura, H. Fujimoto, and M. Fujitsuma, "Torque ripple suppression control for PM motor with current control based on PTC," in *Proc. of the International Power Electronics Conference (IPEC)*, 2010.

[36] K. M. Le, H. V. Hoang, and J. W. Jeon, "An advanced closed-loop control to improve the performance of hybrid stepper motors," *IEEE Transactions on Power Electronics*, vol. 32, no. 9, pp. 7244–7255, 2017.

[37] B. Francis and W. Mohan., "Internal model principle in control theory," *Automatica*, vol. 12, pp. 457–465, 1976.

[38] A. Vidal, F. Freijedo, A. Yepes, P. Fernández, J. Malvar, O. Lopez, and J. Doval-Gandoy, "Assessment and optimization of the transient response of proportional-resonant current controllers for distributed power generation systems," *IEEE Transactions on Industrial Electronics*, vol. 60, no. 4, pp. 1376–1383, 2013.

[39] G. Shen, X. Zhu, J. Zhang, and D. Xu., "A new feedback method for PR current control of LCL-filter-based grid-connected inverter," *IEEE Transactions on Industrial Electronics*, vol. 57, no. 6, pp. 2033–2041, 2010.

[40] M. Bodson, A. Sacks, and P. Khosla, "Harmonic generation in adaptive feedforward cancellation schemes," *IEEE Transactions on Automatic Control*, vol. 39, no. 9, pp. 1939–1944, 1994.

[41] S. Malo and R. Griñó, "Adaptive feed-forward cancellation control of a full-bridge dc-ac voltage inverter," in *Proc. of the 17th IFAC World Congress*, 2008, pp. 4571–4576.

[42] D. Zmood and D. Holmes, "Stationary frame current regulation of PWM inverters with zero steady-state error," *IEEE Transactions on Power Electronics*, vol. 18, no. 3, pp. 814–822, 2003.

[43] M. F. Byl, S. J. Ludwick, and D. L. Trumper, "A loop shaping perspective for tuning controllers with adaptive feedforward cancellation," *Precision Engineering*, vol. 29, no. 1, pp. 27–40, 2005.

[44] A. Arias, J. Caum, and R. Griñó, "Moving towards the maximum speed in stepping motors by means of enlarging the bandwidth of the current controller," *Mechatronics*, vol. 40, pp. 51–62, 2016.

[45] C. L. Phillips, H. T. Nagle, and A. Chakrabortty, *Digital Control Systems Analysis & Design*. Pearson Education Limited, 2014.

[46] N. Mohan, *Electric Machines and Drives: A First Course*. Wiley, 2012.

Antoni Arias received the B.Eng. degree in electrical engineering, and the M.Eng. and Ph.D. degrees in control and electronic engineering from the Universitat Politècnica de Catalunya (UPC), Catalonia, Spain, in 1993, 1997, and 2001, respectively. From 1992 to 1995, he worked at a local industrial electronics company. Since 1996, he has been a Lecturer at the UPC and was appointed as an Associate Professor in 2002. In 1999, he was a Visiting Research Assistant and a part time lecturer at the University of Glamorgan, U.K. In 2003-2004, he joined as a Visiting Fellow in the PEMC Group at the University of Nottingham, U.K. In 2011-2012, he was an MCF invité at the GeePs, France. His research interests include sensorless variable-speed drive systems, power electronics converters, and control strategies.

Jesús Caum received the BEng in electrical engineering, MEng in control and electronic engineering and PhD in optics engineering from the Universitat Politècnica de Catalunya (UPC), Catalonia, Spain, in 1987, 1998 and 2010 respectively. Since 1987 he has been a Lecturer at the Universitat Politècnica de Catalunya and was appointed as an Associate Professor in 1992 at the same University. He is also a member of the CD6 (Centre Development Sensors and Systems) of the UPC since 1995, where he participates and develops industrial projects. In 2006 he started a collaboration with the company MicroPap Easy Motion devoted to the design and development of stepper motor drivers. His research interests include design of conditioning circuits for electro optics sensors and control strategies applied to stepper motors.

Edorta Ibarra received the first M.Sc. degree in electronic engineering from the University of the Basque Country, Bilbao, Spain, in 2004, the second M.Sc. degree in electronic physics from the University of Cantabria, Santander, Spain, in 2005, and the Ph.D. degree in power electronics from the University of the Basque Country, in 2011. During 2006 to 2007, he was with the Technical Engineering School of Bilbao, Spain. From 2007 to 2014, he was with the Applied Electronic Research Group, University of the Basque Country. From 2014 to 2016, he was with Tecnalia Research & Innovation, Industry and Transport Unit, Derio, Spain. Since 2016, he has been an Assistant Professor in the Department of Electronic Technology, University of the Basque Country. His current research interests include power electronics and electrical machine control for automotive and aeronautical applications.

Robert Griñó received the M.Sc. degree in electrical engineering and the Ph.D. degree in automatic control from the Universitat Politècnica de Catalunya (UPC), Barcelona, Spain, in 1989 and 1997, respectively. From 1990 to 1991, he was a Research Assistant with the Instituto de Cibernética, UPC. From 1992 to 1998, he was an Assistant Professor with the Automatic Control Department, Universitat Politècnica de Catalunya, where he has been an Associate Professor since 1998. His research interests include digital control, nonlinear control and control of power electronic converters. Dr. Griñó is an affiliate member of International Federation of Automatic Control (IFAC) and a member of the Spanish Society on Automation and Control-IFAC.